Author Manuscript

Author Manuscript

Author Manuscript

Author Manuscript

HHS Public Access

Author manuscript

Mol Imaging Biol. Author manuscript; available in PMC 2019 June 18.

Published in final edited form as:

Mol Imaging Biol. 2019 June ; 21(3): 417–425. doi:10.1007/s11307-019-01348-z.

Optical Redox Imaging of Fixed Unstained Muscle Slides Reveals Useful Biological Information

He N. Xu[1,2,3,4], **Huaqing Zhao**[5], **Karthikeyani Chellappa**[6], **James G. Davis**[6], **Shoko Nioka**[1,2], **Joseph A. Baur**[6], and **Lin Z. Li**[1,2,3,4]

[1]Department of Radiology, Perelman School of Medicine, University of Pennsylvania, Philadelphia, PA, USA

[2]Department of Biochemistry and Biophysics, Britton Chance Laboratory of Redox Imaging, Johnson Research Foundation, Perelman School of Medicine, University of Pennsylvania, Philadelphia, PA, USA

[3]Institute of Translational Medicine and Therapeutics, Perelman School of Medicine, University of Pennsylvania, Philadelphia, PA, USA

[4]Abramson Cancer Center, University of Pennsylvania, Philadelphia, PA, USA

[5]Department of Clinical Sciences, Temple University School of Medicine, Philadelphia, PA, USA

[6]Department of Physiology, Institute for Diabetes, Obesity, and Metabolism and University of Pennsylvania, Philadelphia, PA, USA

Abstract

Purpose: Optical redox imaging (ORI) technique images cellular autofluorescence of nicotinamide adenine dinucleotide (NADH) and oxidized flavoproteins (Fp containing FAD, *i.e.,* flavin adenine dinucleotide). ORI has found wide applications in the study of cellular energetics and metabolism and may potentially assist in disease diagnosis and prognosis. Fixed tissues have been reported to exhibit autofluorescence with similar spectral characteristics to those of NADH and Fp. However, few studies report on quantitative ORI of formalin-fixed paraffin-embedded (FFPE) unstained tissue slides for disease biomarkers. We investigate whether ORI of FFPE unstained skeletal muscle slides may provide relevant quantitative biological information.

Procedures: Living mouse muscle fibers and frozen and FFPE mouse muscle slides were subjected to ORI. Living mouse muscle fibers were imaged *ex vivo* before and after paraformaldehyde fixation. FFPE muscle slides of three mouse groups (young, mid-age, and muscle-specific overexpression of nicotinamide phosphoribosyltransferase (Nampt) transgenic mid-age) were imaged and compared to detect age-related redox differences.

Results: We observed that living muscle fiber and frozen and FFPE slides all had strong autofluorescence signals in the NADH and Fp channels. Paraformaldehyde fixation resulted in a

Correspondence to: He Xu; hexu2@pennmedicine.upenn.edu, Lin Li; linli@pennmedicine.upenn.edu.

Compliance with Ethical Standards

Conflict of Interest

The authors declare that they have no conflict of interest.

Author Manuscript Author Manuscript Author Manuscript Author Manuscript

significant increase in the redox ratio Fp/(NADH + Fp) of muscle fibers. Quantitative image analysis on FFPE unstained slides showed that mid-age gastrocnemius muscles had stronger NADH and Fp signals than young muscles. Gastrocnemius muscles from mid-age Nampt mice had lower NADH compared to age-matched controls, but had higher Fp than young controls. Soleus muscles had the same trend of change and appeared to be more oxidative than gastrocnemius muscles. Differential NADH and Fp signals were found between gastrocnemius and soleus muscles within both mid-aged control and Nampt groups.

Conclusion: Aging effect on redox status quantified by ORI of FFPE unstained muscle slides was reported for the first time. Quantitative information from ORI of FFPE unstained slides may be useful for biomedical applications.

Keywords

NADH and flavoproteins containing FAD; Redox ratio; Autofluorescence; Formalinfixed unstained tissue slide; Muscle aging

Introduction

Fluorescence properties of mitochondrial nicotinamide adenine dinucleotide (NADH) and oxidized flavoproteins (Fp containing FAD, *i.e.,* flavin adenine dinucleotide) contain a wealth of information on the metabolic status of a living system. Optical redox imaging (ORI) probes metabolic/redox status based on imaging the autofluorescence of endogenous NADH and Fp, and calculating the Fp redox ratio Fp/(NADH+Fp). Pioneered by Chance et al. [1–5], ORI has been widely applied to investigate cell/tissue energetics and metabolism for acquiring biological and pathological information and detecting therapeutic response [6–23]. For example, by ORI of the snap-frozen core biopsies from clinical breast cancer patients, we discovered that compared to normal surrounding tissues, cancerous breast tissues have higher Fp and NADH signals and a higher Fp redox ratio Fp/(NADH+Fp), indicating a more oxidized state [9]. We also found in breast tumor xenografts models that the highly metastatic tumor MDA-MB-231 has a higher level of redox heterogeneity with localized regions of higher redox ratio compared to the less metastatic tumor MCF-7 [12]. We observed that the Fp redox ratio of the more oxidized intratumor subpopulations significantly and linearly correlated with the invasive potential of five mouse xenograft models of human melanomas spanning a full range of metastatic potential [11]. These studies were all performed with snap-frozen tissues. Snap-freezing is a standard preparation procedure that rapidly arrests tissue metabolism and preserves, as closely as possible, the metabolic state of a fresh tissue [24].

Beside snap-freezing, tissue fixation with formalin or other fixation reagents is another way of preventing tissue from decaying. Multiple studies have shown that the characteristic peaks of NADH and Fp persist and the fundamental properties of their endogenous fluorescence are preserved during formalin fixation followed by paraffin embedding process [25–29]. Thus, measuring the fluorescence signals of NADH and Fp channels in FFPE unstained tissue may reveal biologically and pathologically relevant information. For example, using a spectroscopic approach, Majumder et al. found that significant differences are detected in formalin-fixed slides derived from cancerous breast tissue and normal surrounding tissue,

Author Manuscript Author Manuscript Author Manuscript Author Manuscript

with the cancerous tissue having higher signal in the spectral range of NADH fluorescence [26]. This is consistent with our findings on snap-frozen tissues from clinical breast cancer patients [9]. Conklin et al. investigated fixed unstained tissue slides from a transgenic mouse model of breast carcinoma *in situ* consisting of both cancerous and normal tissues employing multiphoton excitation and photon-counting techniques [28]. They observed that the cancerous tissue had higher FAD (Fp) intensity compared to the normal regions. Xu et al. mapped the nominal concentrations of various endogenous fluorophores including NADH and FAD (Fp) in an FFPE unstained tissue matrix array using a wide field fluorescence microscope. They found that the concentrations of these fluorophores significantly decreased from normal, perilesional, to cancerous lung tissue [29]. It has also been reported that formalin has a relatively weak effect on the fluorescence spectrum in the signal range of NADH and Fp compared to methanol which increases the fluorescence signal of NADH channel [27]. These studies indicated a potential for applying ORI to FFPE unstained tissue slides using a regular wide field fluorescence microscope. Such a technique can be useful to acquire pathological information from clinically annotated FFPE slides which are readily available.

Our long-term goal is to investigate whether ORI technique can be applied to quantitatively image clinical FFPE unstained tissue slides to extract pathological information for cancer diagnosis/prognosis. Some preliminary data showing ORI of FFPE slides of breast tumors (both animal model and tumor tissue from clinical patients) have been published in a conference proceedings [30]. Considering the high complexity of tumor tissues, we started with a relatively simpler model: mouse skeletal muscle tissue slides for quantitative analysis of imaging data. Since we have not seen any imaging study that reports the immediate fixation effect on tissue NADH and Fp fluorescence signals, we first show the quantitative changes of ORI indices induced by paraformaldehyde (PFA) on fresh muscle fibers. We then report quantitative analysis on ORI of FFPE unstained muscle slides of three mouse groups (young, mid-age, and mid-age Nampt). Finally, we discuss some technical issues and future development of this technique. To our knowledge, ORI of FFPE unstained muscle slides to quantify aging effect on the redox status has not been reported before.

Materials and Methods

The animal protocols utilized in the study were approved by the Institutional Animal Care and Use Committee of the University of Pennsylvania.

Imaging Fixation Effect

To investigate the fixation effect on redox indices, living mouse muscle fiber bundles of < 1 mm thick were isolated from 16-week-old C57BL/6J.Nia mice immediately after cervical dislocation and placed into oxygenated Ringer's solution in a 35-mm glass-bottom Petri dish. They were imaged within 30 min using a Leica SP8 Multiphoton Microscope (NADH channel: 750-nm excitation and 435–485-nm emission, Fp channel: 860-nm excitation and 515–535-nm emission). Some leg muscles of 1–3 mm thick were also isolated from an anesthetized male nude mouse and placed in PBS spiked with 25 mM glucose. They were imaged within 30 min using an EVOS FL Auto Imaging microscope with filter cubes of

Author Manuscript Author Manuscript Author Manuscript Author Manuscript

DAPI (357/44 nm excitation, 447/60 nm emission) and GFP (470/22 nm excitation, 510/42 nm emission). Immediately after imaging, the media were changed to 4 % PFA on site without removing the Petri dish off the microscope stage in order to keep the specimen at its original *x*-*y* position. Approximately 5–10 min later, the same field of view (FOV) was imaged again. A single location/FOV was imaged once for any particular sample both before and after PFA fixation.

Imaging Tissue Slides

Frozen Muscle Slides—C57BL/6J.Nia young (3 months) and old (20 months) male mice were sacrificed by cervical dislocation and dissected gastrocnemius muscles were immediately frozen in OCT under chilled isopentane and stored in – 80 °C. Muscle slides of 30 μm thickness were obtained by cryosectioning the tissue blocks (– 20 °C) and stored in – 20 °C freezer until imaging. Right before imaging, a drop of chilled PBS was placed on the frozen slide followed by covering with a cover glass. The slide was then immediately placed in the imaging chamber and imaged with the EVOS FL Auto Imaging microscope under room temperature. The time duration between the frozen state and imaging was a couple of minutes.

FFPE Muscle Slides—FFPE slides were prepared from three groups of C57BL/ 6J.Nia mice. The young group includes three 14-week-old mice. The mid-age group includes three 13-month-old mice. These two groups are designated as the control groups consisting of Cre only, floxed, or wild-type mice, which are phenotypically identical according to our observation. The third group is the transgenic group which is made of three 13-month-old mice with musclespecific Nampt overexpression [31]. We refer to this group as Nampt group. Gastrocnemius and soleus muscles were immediately isolated from the three groups of mice after cervical dislocation. The isolated muscles were fixed with 4 % PFA in 1× PBS overnight and rinsed in 1× PBS (fixation time ~16 h) followed by changing PBS six to eight times until paraffin embedding next day. Tissue slides were cut with a thickness of 7 μm. Gastrocnemius and soleus muscles from the same mouse were placed on the same slide. All these fixed slides were stored in slide box at room temperature until imaging. The storage time was 5–6 years.

For each group, three FFPE unstained muscle slides (each from an individual mouse) were subjected to ORI using the same EVOS microscope as mentioned above. For each slide, multiple (5–10) randomly selected FOVs were imaged with a 20× objective. Images of the young and mid-age control muscles were acquired within 3 days. The Nampt muscle slides were imaged 30 days later.

Image Analysis

Matlab® routines were used to quantify signal intensities of muscle slides for NADH and Fp channels. Each image was first flattened by fitting the overall background with a third-degree polynomial function (poly33) and subtracting the function from the image. The mean background intensity was then computed by drawing an ROI at a paraffin-covered region where there was no tissue. This mean background was subtracted when calculating the mean values of each FOV. The thresholds of both NADH and Fp signals were three times the

Author Manuscript Author Manuscript Author Manuscript Author Manuscript

background standard deviation above the mean of the background signal. Pixels with signals above the threshold were kept for further data processing. For quantitative comparisons, NADH and Fp signals across different FOVs and slides were all normalized to the same exposure time, instrument gain, and light source intensity. The mean values of each redox index *(i.e.,* Fp, NADH, and the redox ratio Fp/(Fp + NADH)) were obtained for each FOV.

Statistical Analysis

Paired Student's *t* test was performed to identify the PFA effects on the redox indices of living muscle tissues. Images of cross-sectional gastrocnemius and soleus muscle fibers were selected for statistical analysis with linear mixed-effect model (LMM). In the LMM analysis, the "subjects" were mouse ID and "repeated" was FOV with covariance structure of heterogeneous autoregressive; one of the redox indices, *e.g.,* Fp, was set as "dependent variable" for each analysis with group being the "fixed-effect factor." There were three comparisons made between groups (young, mid-age, and Nampt) and one within group (gastrocnemius *vs* soleus) for each redox index, and $p < 0.01$ was considered statistically significant with adjustment for multiple comparisons.

Results

PFA Fixation Effects on the Redox Signals

NADH and Fp florescence signals are readily detectable in muscle tissues and the majority of the NADH and Fp signals come from mitochondria [32–36]. Employing a two-photon microscope, we first imaged several living muscle fiber bundles *ex vivo* and re-imaged the same FOV ~5 min after the medium was replaced with 4 % PFA. Figure 1 shows before and after fixation results of one muscle fiber bundle. In both living and fixed conditions, the fiber bundles exhibit abundant NADH and Fp fluorescence and fixation induced a pronounced increase in Fp signal intensity.

For easier experimental performance, we then employed the EVOS microscope to image four specimens of muscle fiber bundles *ex vivo* before and after PFA fixation acquiring signals from the same FOVs. All of them showed the similar trend of change due to PFA fixation for each redox index as shown in Fig. 2 for the individual samples. Paired *t* test analysis shows that the average Fp signal increased ~40 % *(*$p = 0.095$), the average NADH signal decreased ~13 % *(*$p = 0.17$), and the average Fp redox ratio was 15 % higher *(*$p = 0.0093$) after fixation (Fig. 2). It appears that for leg muscle, PFA affected the Fp signal more than it did the NADH intensity, resulting in a significantly higher redox ratio.

Quantitative Analysis on ORI of FFPE Muscle Slides

To ensure that we can detect NADH and Fp signals of muscle slides, we first imaged several frozen muscle slides at room temperature. Figure 3 shows redox images of a young and an old muscle section. To better display the fine structures of the fibers, the color bar scales of Fp and NADH images of the young muscle slide were set half of that for the old muscle. In the section of young muscle, three fiber types as represented by the different intensities [37] can be identified: bright, mid-level, and low level of brightness in both Fp and NADH images. In the old muscle section, the average signal intensities in both channels were higher

Author Manuscript Author Manuscript Author Manuscript Author Manuscript

than that of the young muscle, but the contrast among fiber types diminished and the intensity inside individual fibers decreased while the fiber rim became brighter. To detect possible signal changes of the frozen slides over time, for one of the slides we also imaged the same FOV at different time points starting from 4 to 40 min at approximately 10- min intervals. We found that NADH decreased ~14 % and Fp increased ~7 % over the time course of ~40 min.

Since we were able to readily detect NADH and Fp signals from living muscle fibers before and after fixation, and frozen muscles on glass slide, we then performed ORI of FFPE unstained muscle slides of different mouse ages to investigate whether the redox indices could detect age difference. Typical ORI images are shown in Fig. 4. In the young gastrocnemius muscle, the different types of fiber are clearly observed, more prominent in Fp and redox ratio images. The boundary of the fibers of the mid-age gastrocnemius muscle is less clearly defined. However, the boundary of Nampt gastrocnemius muscle fibers appear to be better defined than that of the control mid-age gastrocnemius muscle. Similarly, different fiber types are also observable in the images of soleus muscle.

To test if the quantitative redox indices obtained from imaging the FFPE unstained slides can differentiate among three muscle groups, we quantified the mean values of NADH, Fp, and the redox ratio in each FOV image. Boxplots for the redox index measurements of individual fields of view were shown in Fig. 4. We performed LMM analyses to compare the redox difference among three groups. As shown in Table 1, for the gastrocnemius muscle slides, either Fp or NADH intensity readily distinguished the young group from the mid-age group with the young muscle fibers having significantly lower Fp and NADH. The values of Fp and NADH of Nampt group fall in between and significantly differ from the young and mid-age groups. The redox ratio was not significantly different among three groups.

A similar trend of changes was also observed for the soleus muscles. The mid-age soleus muscles have significantly larger NADH compared to the young group. NADH and Fp intensities of Nampt group again fall in between that of the other two groups, with NADH being significantly lower than that of age-matched control fibers. Similar to the gastrocnemius muscles, there was no significant difference in the redox ratio among the three groups.

We also compared gastrocnemius with soleus muscles within the same age group. We found that soleus muscles have higher redox ratio than gastrocnemius muscles for the young group with a marginal significance ($p = 0.016$) but neither Fp nor NADH differs significantly. For the mid-age group, soleus muscles are higher in NADH ($p = 0.011$), Fp ($p = 0.034$), and the redox ratio ($p = 0.0003$) than gastrocnemius muscles. For Nampt group, soleus muscles are higher in both NADH ($p = 0.024$) and Fp ($p = 0.0074$) than gastrocnemius muscles with the redox ratio trending higher ($p = 0.20$). Overall, soleus muscles have a trend of being more oxidative and higher in NADH and Fp than gastrocnemius muscles. The higher fluorescence signal intensities in the more oxidative soleus muscles may reflect its higher mitochondrial content [38].

Author Manuscript Author Manuscript Author Manuscript Author Manuscript

Discussion

This paper reports initial quantitative results for a feasibility study aiming to develop an ORI technique for imaging FFPE unstained tissue slides to identify potential optical biomarkers. It is known that formaldehyde changes the molecular properties of tissues, such as attaching hydroxyl-methyl groups to these molecules, which may react with other molecules to form crosslinks in a complex manner [39]. Prior reports indicate that formalin fixation results depend on the types of tissue specimens and how they were stored. The spectroscopic study by Filippidis et al. shows that formalin fixation increases the fluorescence intensity of calcified plaque in the spectral range of Fp [25]. Majumder et al. reported that in the spectral range of NADH and Fp fluorescence, formalin fixation caused no noticeable change in spectral intensity of normal breast tissue but a large increase in breast cancer tissue [26]. This differential effect of formalin fixation was explained by breast cancer tissue having higher water and hemoglobin content which were lost during fixation. Furthermore, Conklin et al. reported a quantitative comparison between live and fixed 3D models of normal human breast cell line MCF10A [28]. Their findings show that fixation did not significantly change the fluorescence lifetimes of NADH and Fp (in either bound or free form) in the acini. In the present study, we monitored both NADH and Fp signals for the same location/FOV of living muscle fibers before and immediately after ~5 min PFA fixation. We observed a 15 % increase of redox ratio due to fixation. The statistically insignificant changes of Fp and NADH caused by immediate PFA fixation are likely due to the large inter-tissue standard deviations. We have not seen any reported comparison of NADH and Fp fluorescence intensities between living and PFA fixed muscle tissues. More repeated experiments are needed to verify the preliminary results reported here.

By ORI of both frozen and fixed muscle slides, we observed distinct types of muscle fibers based on fiber fluorescence intensities in the NADH and Fp channels. Such imaging patterns of muscle autofluorescence attributable to NADH and Fp fluorophores have also been observed in fixed or frozen slides of mouse or monkey skeletal muscles by others [40, 41]. These patterns were associated with various fiber types exhibiting different mitochondrial activities. However, there were no previous reports on such redox heterogeneity patterns of FFPE unstained muscle slides as we presented here.

By quantifying Fp and NADH signals, we also showed that mid-age and old muscles had overall higher Fp and NADH intensities than those from young mice, indicative of higher contents of Fp and NADH. Although the NAD^+ pool has been reported to decrease with age in muscle [42], several studies have reported a redox shift and/or increase in NADH that is consistent with our findings. For example, using a fluorescence microscope to measure NADH intensity in living lumbrical muscles of mouse hind paw, Claflin et al. found an age-associated elevation of NADH [37] and Braidy et al. reported a shift in the NAD^+/NADH redox state favoring NADH in multiple tissues of aged rats [43]. Employing a two-photon imaging system, Pugh et al. observed an elevated FAD in mid-age (15 years old) skeletal muscle (vastus lateralis) of rhesus monkeys, and the free NAD^+/NADH ratio as biochemically measured from the muscle homogenates decreased in mid-age muscle compared to both young and old [41]. A more reduced mitochondrial redox environment with increased NADH autofluorescence in old mice has also been reported by others [44]. In

Author Manuscript Author Manuscript Author Manuscript Author Manuscript

addition to Fp and NADH intensities, we also quantified the Fp redox ratio which showed no significant difference between young and mid-age groups. Further investigations are needed to confirm whether and how the Fp redox ratio may change with age.

Nampt is the rate-limiting enzyme in the salvage pathway for NAD synthesis from nicotinamide, which is the dominant pathway in skeletal muscle. NAD concentration decreases in muscle over the course of natural aging and increasing NAD synthesis has been suggested to delay some age-related degenerative processes [42]. Our data showed that mid-age muscles had significantly higher NADH than young muscles. Consistently, we observed that Nampt overexpressed muscles had significantly lower NADH than that of aged-matched control muscles.

Compared to spectroscopy, imaging/scanning techniques are advantageous for studying tissues since both signal intensity and spatial heterogeneity can be obtained. With the Chance redox scanner being a standard technique/tool in our research, raster scanning of snap-frozen tissues immersed in liquid nitrogen allows us to extract both intensity and spatial heterogeneity information at a resolution of ~50–200 μm. When taking spatial redox heterogeneity into account, we found intra-tissue heterogeneity-associated redox indices readily differentiated tumors with different metastatic potentials [11, 12] or genetic status [45, 46], whereas the difference was not or less significant by global averaging method. The submillimeter spatial heterogeneity information revealed by redox scanning/imaging would be difficult to obtain by spectroscopy.

On the other hand, the Chance redox scanner is still limited by its spatial resolution of 50 μm. The much higher resolution (~1 μm) achieved by a fluorescence microscope may serve the purpose of identifying redox information on a finer scale. In the case of studying muscles, the redox information of the fine structures of a fiber bundle (diameter ~50 μm) can be readily revealed by a fluorescence microscope (Figs. 3 and 4). We can observe different fiber types and segment fiber types to determine how aging may have affected them individually, although we only performed global averaging of redox indices for the purpose of this study. To our knowledge, quantitative ORI analysis of FFPE unstained muscle slides based on individual fiber types have not been reported and could be a direction of future investigation.

Several technical issues should be addressed in the future. We need to have better controlled fixation process to study fixation effects on the intensity of NADH and Fp with various types of tissues. In the present study, we also imaged two fixed slides of adjacently cut young gastrocnemius muscle and found that the mean values of the redox indices were very close (data not shown), supporting the reproducibility of this technique for imaging FFPE slides. For method validation, the reproducibility of imaging fixed tissue slides should be further evaluated. Longitudinal ORI should be performed on tissue slides to test whether there is a temporal dependence of ORI signals of FFPE unstained tissue slides. In addition, an internal standard may be needed to account for instrument fluctuations across different imaging sessions (although the possible instrument fluctuation was insignificant within the short period of this study). An imaging analysis method that removes the vignette effect for quantification of fluorescence intensity of entire tissue slides may also be needed should tile-

Author Manuscript Author Manuscript Author Manuscript Author Manuscript

imaging is used to image a large tissue area on the slide. To screen large quantities of clinical tissue slides, our image analysis method needs improvement in its versatility, such as removing artifacts and extracting pathologically relevant information.

Conclusions

This study investigates the feasibility of ORI of FFPE unstained skeletal muscle slides to quantify aging effect on the redox status. PFA fixation of living mouse leg muscle resulted in a higher Fp redox ratio but insignificant change in NADH and Fp. Distinct muscle fiber types and fine fiber structures based on the fluorescence intensity have been observed in both frozen and FFPE slides. We discovered that mid-age gastrocnemius muscles had significantly higher signals in both NADH and Fp channels than the corresponding young muscles. Nampt-overexpressed transgenic gastrocnemius muscles showed intermediate NADH signals compared to those of young *vs* age-matched control muscles. We found no significant difference in the Fp redox ratio among three groups. We also observed that the Fp redox ratio of soleus muscles was significantly higher than gastrocnemius muscles in the mid-age group and trending higher in both the young and Nampt groups. The NADH and Fp signals in the soleus muscles tend to be higher than those in the gastrocnemius muscles. Although more experiments are needed to further develop this approach, the ORI patterns of muscle fibers and quantitative analysis on aging effects shown in this study reveal the potential of this technique to provide biological and pathologically relevant information.

Acknowledgements.

We thank Dr. William Quinn for providing the living muscle samples, Annemarie Jacob for her assistance during imaging the fixation effects, and Dr. Gordon Ruthel for his assistance in two-photon imaging. We also thank the Cell and Developmental Biology (CDB) Microscopy Core, Perelman School of Medicine and Penn Vet Imaging Core, School of Veterinary Medicine, University of Pennsylvania.

*Funding Information.*This work was supported by the NIH Grants R01CA191207 (L.Z. Li) and R01 DK098656 (J. A. Baur) and a pilot grant (L.Z. Li and J. A. Baur) from the University of Pennsylvania Institute on Aging.

References

1. Chance B, Baltscheffsky H (1958) Respiratory enzymes in oxidative phosphorylation. VII Binding of intramitochondrial reduced pyridine nucleotide. J Biol Chem 233:736–739 [PubMed: 13575447]
2. Chance B, Schoener B (1966) Fluorometric studies of flavin component of the respiratory chain In: Slater EC (ed) Flavins and flavoproteins. Elsevier, New York, pp 510–519
3. Chance B, Cohen P, Jobsis F, Schoener B (1962) Intracellular oxidation-reduction states in vivo. Science 137:499–508 [PubMed: 13878016]
4. Chance B, Schoener B, Oshino R, Itshak F, Nakase Y (1979) Oxidation-reduction ratio studies of mitochondria in freeze-trapped samples. NADH and flavoprotein fluorescence signals. J Biol Chem 254:4764–4771 [PubMed: 220260]
5. Quistorff B, Haselgrove JC, Chance B (1985) High spatial resolution readout of 3-D metabolic organ structure: an automated, low-temperature redox ratio-scanning instrument. Anal Biochem 148:389–400 [PubMed: 4061818]
6. Georgakoudi I, Quinn KP (2012) Optical imaging using endogenous contrast to assess metabolic state. Annu Rev Biomed Eng 14:351–367 [PubMed: 22607264]
7. Xu HN, Li LZ (2014) Quantitative redox imaging biomarkers for studying tissue metabolic state and its heterogeneity. J Innov Opt Health Sci 7:1430002

Author Manuscript Author Manuscript Author Manuscript Author Manuscript

8. Xu HN, Feng M, Nath K, Nelson D, Roman J, Zhao H, Lin Z, Glickson J, Li LZ (2018) Optical redox imaging of lonidamine treatment response of melanoma cells and xenografts. Mol Imaging Biol. 10.1007/s11307-018-1258-z
9. Xu HN, Tchou J, Feng M, Zhao H, Li LZ (2016) Optical redox imaging indices discriminate human breast cancer from normal tissues. J Biomed Opt 21:114003
10. Kirkpatrick ND, Brewer MA, Utzinger U (2007) Endogenous optical biomarkers of ovarian cancer evaluated with multiphoton microscopy. Cancer Epidemiol Biomark Prev 16:2048–2057
11. Li LZ, Zhou R, Xu HN, Moon L, Zhong T, Kim EJ, Qiao H, Reddy R, Leeper D, Chance B, Glickson JD (2009) Quantitative magnetic resonance and optical imaging biomarkers of melanoma metastatic potential. Proc Natl Acad Sci U S A 106:6608–6613 [PubMed: 19366661]
12. Xu HN, Nioka S, Glickson JD, Chance B, Li LZ (2010) Quantitative mitochondrial redox imaging of breast cancer metastatic potential. J Biomed Opt 15:036010
13. Sun N, Xu HN, Luo Q, Li LZ (2016) Potential indexing of the invasiveness of breast cancer cells by mitochondrial redox ratios. Adv Exp Med Biol 923:121–127 [PubMed: 27526133]
14. Alhallak K, Rebello LG, Muldoon TJ, Quinn KP, Rajaram N (2016) Optical redox ratio identifies metastatic potential-dependent changes in breast cancer cell metabolism. Biomed Opt Express 7:4364–4374 [PubMed: 27895979]
15. Xu HN, Zhao H, Mir TA et al. (2013) CHOP therapy induced mitochondrial redox state alteration in non-Hodgkin's lymphoma xenografts. J Innov Opt Health Sci 6:1350011
16. Shah AT, Beckler MD, Walsh AJ et al. (2014) Optical metabolic imaging of treatment response in human head and neck squamous cell carcinoma. PLoS One 9:e90746
17. Walsh AJ, Cook RS, Sanders ME, Aurisicchio L, Ciliberto G, Arteaga CL, Skala MC (2014) Quantitative optical imaging of primary tumor organoid metabolism predicts drug response in breast cancer. Cancer Res 74:5184–5194 [PubMed: 25100563]
18. Walsh AJ, Cook RS, Manning HC, Hicks DJ, Lafontant A, Arteaga CL, Skala MC (2013) Optical metabolic imaging identifies glycolytic levels, subtypes, and early-treatment response in breast cancer. Cancer Res 73:6164–6174 [PubMed: 24130112]
19. Alam SR, Wallrabe H, Svindrych Z, Chaudhary AK, Christopher KG, Chandra D, Periasamy A (2017) Investigation of mitochondrial metabolic response to doxorubicin in prostate cancer cells: an NADH, FAD and tryptophan FLIM assay. Sci Rep 7:10451 [PubMed: 28874842]
20. Kirkpatrick ND, Zou C, Brewer MA, Brands WR, Drezek RA, Utzinger U (2005) Endogenous fluorescence spectroscopy of cell suspensions for chemopreventive drug monitoring. Photochem Photobiol 81:125–134 [PubMed: 15535738]
21. Ramanujam N, Richards-Kortum R, Thomsen S, Mahadevan-Jansen A, Follen M, Chance B (2001) Low temperature fluorescence imaging of freeze-trapped human cervical tissues. Opt Express 8:335–343 [PubMed: 19417824]
22. Ostrander JH, McMahon CM, Lem S et al. (2010) Optical redox ratio differentiates breast cancer cell lines based on estrogen receptor status. Cancer Res 70:4759–4766 [PubMed: 20460512]
23. Skala M, Ramanujam N (2010) Multiphoton redox ratio imaging for metabolic monitoring in vivo. Methods Mol Biol 594:155–162 [PubMed: 20072916]
24. Lowry OH, Passonneau JV (1972) Chapter 7—preparation of tissues for analysis In: Lowry OH, Passonneau JV (Eds) A flexible system of enzymatic analysis. Academic Press, pp 120–128
25. Filippidis G, Zacharakis G, Katsamouris A, Giannoukas A, Kouktzela M, Papazoglou TG (1998) Effect of liquid-nitrogen and formalinbased conservation in the in vitro measurement of laser-induced fluorescence from peripheral vascular tissue. J Photochem Photobiol B 47:109–114 [PubMed: 10093910]
26. Majumder SK, Ghosh N, Gupta PK (2005) N2 laser excited autofluorescence spectroscopy of formalin-fixed human breast tissue. J Photochem Photobiol B 81:33–42 [PubMed: 16107317]
27. Xu MG, Williams ED, Thompson EW, Gu M (2000) Effect of handling and fixation processes on fluorescence spectroscopy of mouse skeletal muscles under two-photon excitation. Appl Opt 39:6312–6317 [PubMed: 18354640]
28. Conklin MW, Provenzano PP, Eliceiri KW, Sullivan R, Keely PJ (2009) Fluorescence lifetime imaging of endogenous fluorophores in histopathology sections reveals differences between

Author Manuscript Author Manuscript Author Manuscript Author Manuscript

normal and tumor epithelium in carcinoma in situ of the breast. Cell Biochem Biophys 53:145–157 [PubMed: 19259625]

29. Xu Z, Reilley M, Li R, Xu M (2017) Mapping absolute tissue endogenous fluorophore concentrations with chemometric wide-field fluorescence microscopy. J Biomed Opt 22:66009 [PubMed: 28617923]
30. Xu HN, Tchou J, Li Y et al. (2018) Optical redox imaging of fixed unstained tissue slides to identify biomarkers for breast cancer diagnosis/prognosis: feasibility study. SPIE BiOS 10472:6
31. Frederick DW, Davis JG, Davila A et al. (2014) Increasing NAD synthesis in muscle via nicotinamide phosphoribosyltransferase is not sufficient to promote oxidative metabolism. J Biol Chem 290:1546–1558 [PubMed: 25411251]
32. Chance B, Connelly CM (1957) A method for the estimation of the increase in concentration of adenosine diphosphate in muscle sarcosomes following a contraction. Nature 179:1235–1237 [PubMed: 13440944]
33. Chance B, Jobsis F (1959) Changes in fluorescence in a frog sartorius muscle following a twitch. Nature 184:195–196
34. Huang S, Heikal AA, Webb WW (2002) Two-photon fluorescence spectroscopy and microscopy of NAD(P)H and flavoprotein. Biophys J 82:2811–2825 [PubMed: 11964266]
35. Blinova K, Levine RL, Boja ES, Griffiths GL, Shi ZD, Ruddy B, Balaban RS (2008) Mitochondrial NADH fluorescence is enhanced by complex I binding. Biochemistry 47:9636–9645 [PubMed: 18702505]
36. Heikal AA (2010) Intracellular coenzymes as natural biomarkers for metabolic activities and mitochondrial anomalies. Biomark Med 4:241–263 [PubMed: 20406068]
37. Claflin DR, Jackson MJ, Brooks SV (2015) Age affects the contraction-induced mitochondrial redox response in skeletal muscle. Front Physiol 6:21 [PubMed: 25698975]
38. Jacobs RA, Diaz V, Soldini L, Haider T, Thomassen M, Nordsborg NB, Gassmann M, Lundby C (2013) Fast-twitch glycolytic skeletal muscle is predisposed to age-induced impairments in mitochondrial function. J Gerontol A-Biol 68:1010–1022
39. Dapson RW (2007) Macromolecular changes caused by formalin fixation and antigen retrieval. Biotech Histochem 82:133–140 [PubMed: 17987439]
40. Jackson KA, Snyder DS, Goodell MA (2004) Skeletal muscle fiber-specific green autofluorescence: potential for stem cell engraftment artifacts. Stem Cells 22:180–187 [PubMed: 14990857]
41. Pugh TD, Conklin MW, Evans TD, Polewski MA, Barbian HJ, Pass R, Anderson BD, Colman RJ, Eliceiri KW, Keely PJ, Weindruch R, Beasley TM, Anderson RM (2013) A shift in energy metabolism anticipates the onset of sarcopenia in rhesus monkeys. Aging Cell 12:672–681 [PubMed: 23607901]
42. Yoshino J, Baur JA, Imai SI (2018) NAD(+) intermediates: the biology and therapeutic potential of NMN and NR. Cell Metab 27:513–528 [PubMed: 29249689]
43. Braidy N, Guillemin GJ, Mansour H, Chan-Ling T, Poljak A, Grant R (2011) Age related changes in NAD^+ metabolism oxidative stress and Sirt1 activity in Wistar rats. PLoS One 6:e19194
44. Mayevsky A, Rogatsky GG (2007) Mitochondrial function in vivo evaluated by NADH fluorescence: from animal models to human studies. Am J Physiol Cell Physiol 292:C615–C640 [PubMed: 16943239]
45. Xu HN, Feng M, Moon L et al. (2013) Redox imaging of the p53- dependent mitochondrial redox state in colon cancer ex vivo. J Innov Opt Health Sci 6:1350016
46. Xu HN, Nioka S, Li LZ (2013) Imaging heterogeneity in the mitochondrial redox state of premalignant pancreas in the pancreasspecific PTEN-null transgenic mouse model. Biomark Res 1:6 [PubMed: 24252270]

Author Manuscript Author Manuscript Author Manuscript Author Manuscript

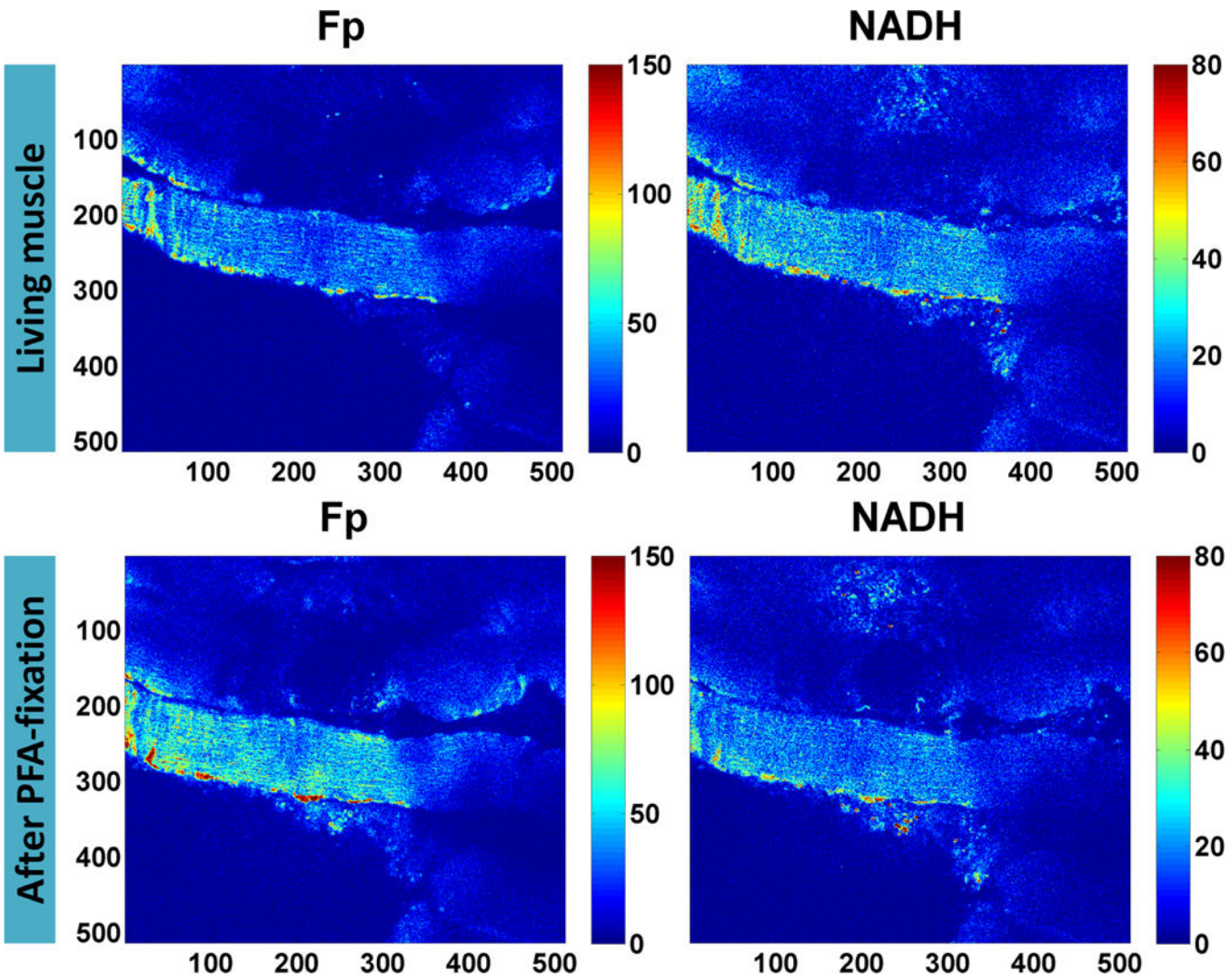

Fig. 1.

Fp and NADH images of muscle fibers before and after PFA fixation (pixel size: 0.72 μm). The intensities are in arbitrary units. The numbers below and on the left side of individual images are the *x* and *y* coordinates of the image matrices. Color bars on the right side of individual images indicate the range of the index being displayed.

Author Manuscript
Author Manuscript
Author Manuscript
Author Manuscript

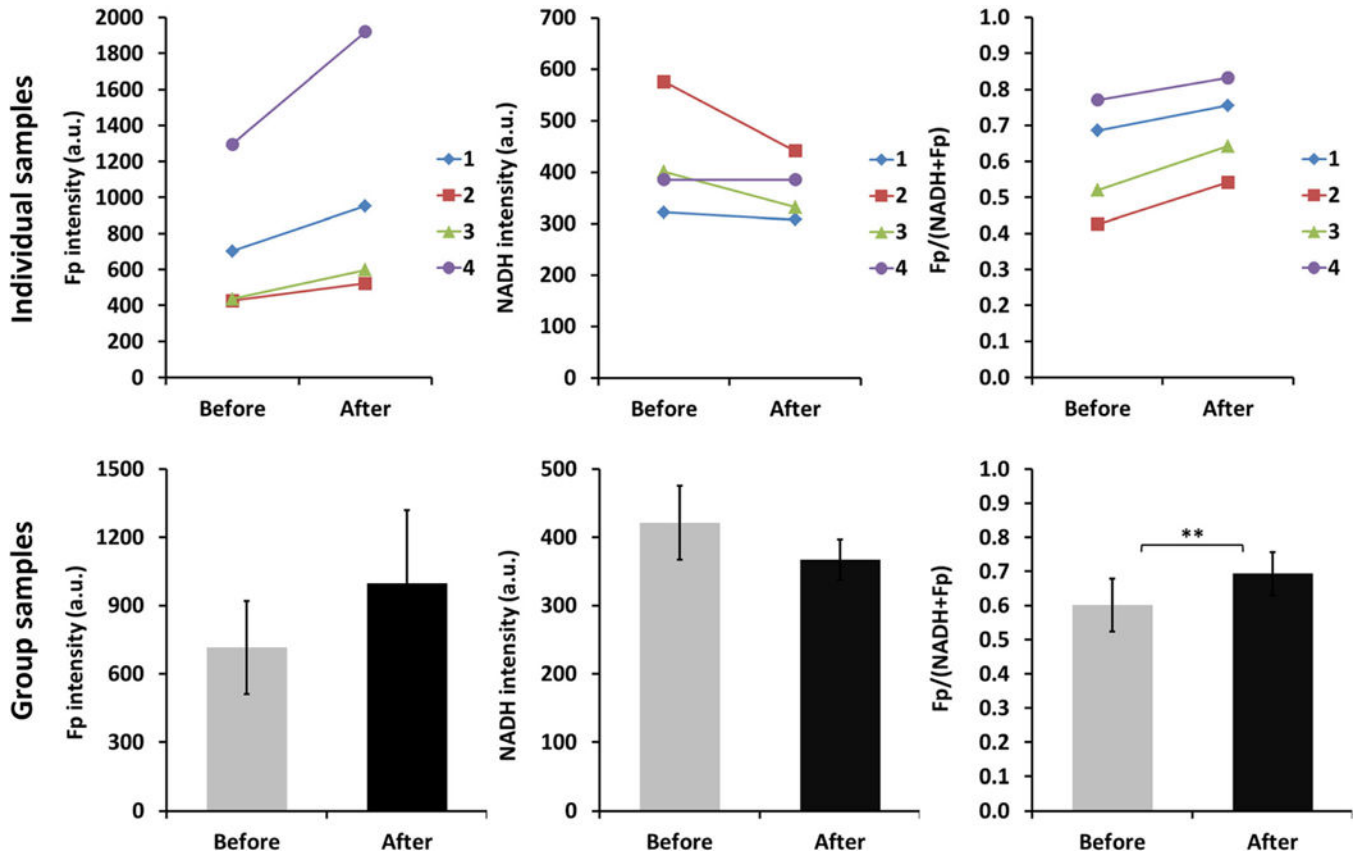

Fig. 2.

The 4 % PFA fixation effect on the redox signals of living muscles of mouse legs ($N = 4$). Number 1, 2, 3, and 4 indicate 4 individual samples and each sample was measured before and after fixation by imaging the same FOV. In the bar graph of group samples, the values are mean ±SE (standard error). ** indicates $p < 0.01$.

Author Manuscript Author Manuscript Author Manuscript Author Manuscript

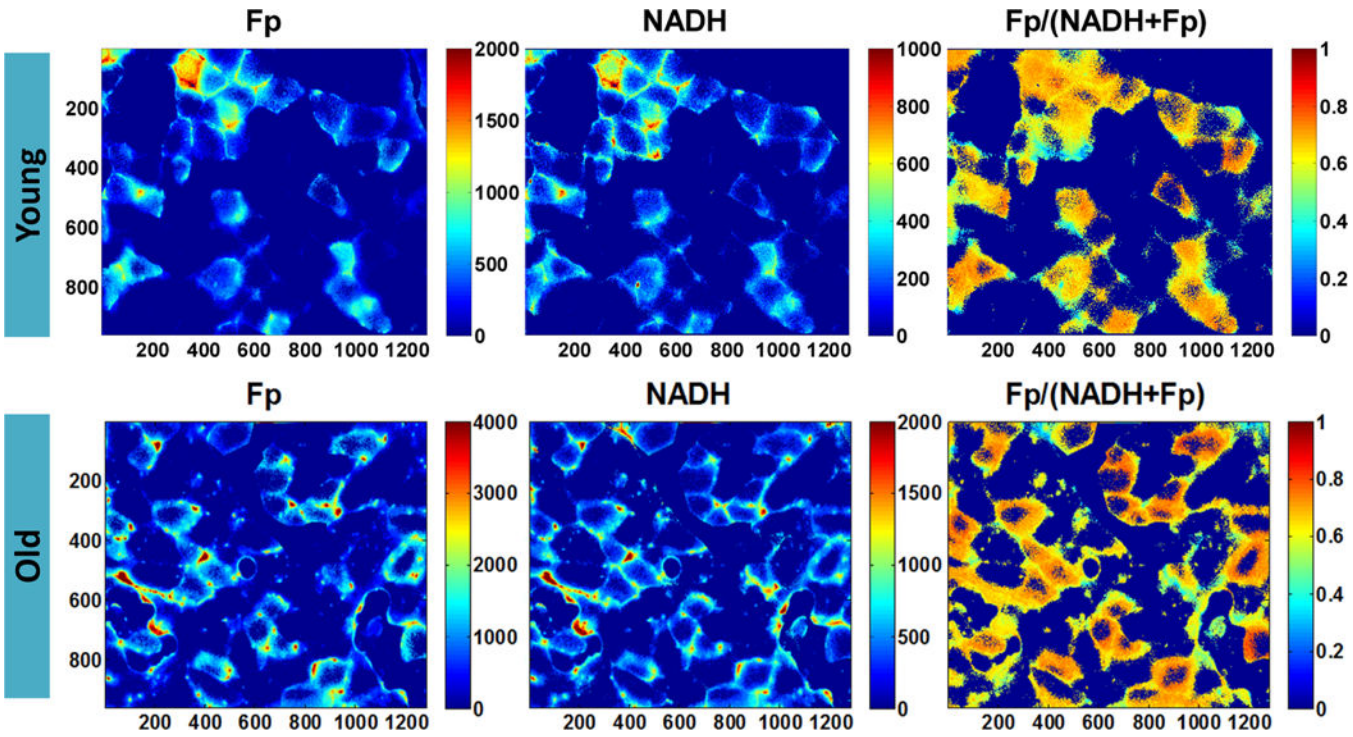

Fig. 3.

Redox images of frozen slides from a young and an old mouse acquired at room temperature (pixel size: 0.35 μm). To better display the fine structures of the fibers, the color bar scales of Fp and NADH images of the young muscle are not set the same as the respective ones of the old muscle.

Author Manuscript
Author Manuscript
Author Manuscript
Author Manuscript

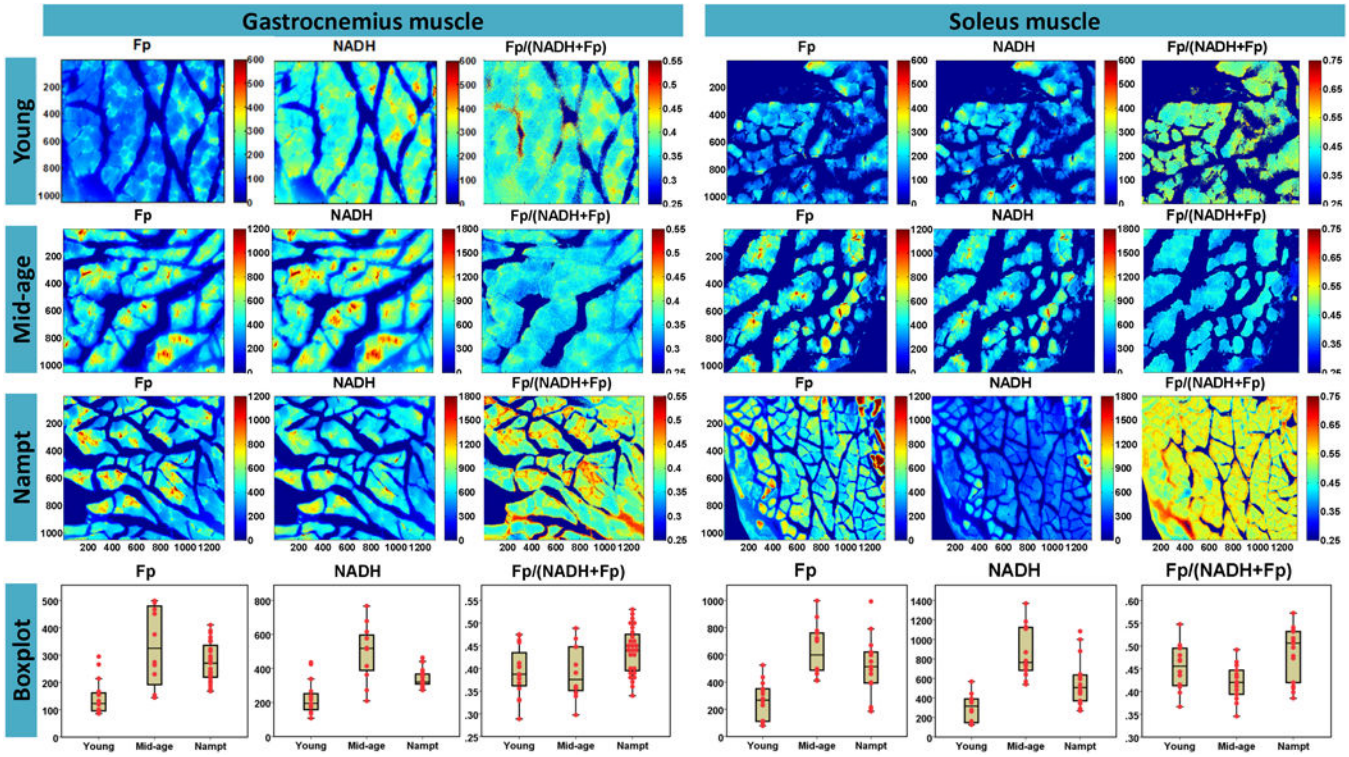

Fig. 4.

Representative redox images of FFPE unstained tissue slides from young and mid-age and Nampt-overexpressed groups (pixel size: 0.35 μm). For the better view of the fine structures, the Fp and NADH color scale bars for the young muscle were set differently from the other two groups. The box of the dotted boxplots indicate the lower adjacent value, first quartile, median, third quartile, and upper adjacent value of the redox indices for a specific group; and the dots represent the mean values of the redox index measurements of individual fields of view.

Author Manuscript Author Manuscript Author Manuscript Author Manuscript

Table 1.

Estimated marginal means ± SE (arbitrary unit) of the redox indices for each group

Group	Gastrocnemius muscle			Soleus muscle		
	Fp	NADH	Fp/(NADH + Fp)	Fp	NADH	Fp/(NADH + Fp)
Young	194 ±24	215 ±27	0.40 ±0.024	317 ± 95	336 ±101	0.44 ±0.027
Mid-age	329 ±24	520±32	0.40 ±0.025	598 ±95	876 ±101	0.44 ±0.027
Nampt	240 ± 23	334±20	0.44 ±0.013	506 ±87	454±89	0.46 ±0.024
P[a]	< 0.0001	< 0.001	> 0.01	>0.01	< 0.01	>0.01
P[b]	< 0.0001	< 0.01	> 0.01	>0.01	< 0.01	>0.01
P[c]	< 0.0001	< 0.01	> 0.01	>0.01	> 0.01	>0.01

[a] Young *vs* mid-age;

[b] Mid-age *vs* Nampt;

[c] Young *vs* Nampt